Science Advances
AAAS

advances.sciencemag.org/cgi/content/full/7/26/eabf5326/DC1

Supplementary Materials for

Sea level and deep-sea temperature reconstructions suggest quasi-stable states and critical transitions over the past 40 million years

Eelco J. Rohling*, Jimin Yu, David Heslop, Gavin L. Foster, Bradley Opdyke, Andrew P. Roberts

*Corresponding author. Email: eelco.rohling@anu.edu.au

Published 25 June 2021, *Sci. Adv* .**7**, eabf5326 (2021)
DOI: 10.1126/sciadv.abf5326

This PDF file includes:

Potential influence of warm, saline deep water
Figs. S1 to S7
Table S1

SUPPLEMENTARY ONLINE MATERIAL

Potential influence of warm, saline deep water

We find no indication of substantial warm and saline deep-water contributions. While such waters would have been warm (causing a tendency to more negative δ_c), they would have also been saline with relatively high δ_w because of evaporation, similar to modern Mediterranean outflow that is 0.5‰ more positive than inflow. For a less extreme concentration effect in a more open setting, smaller offsets are expected, but salinity would then also be less enriched. What matters for a substantial deep-water contribution is the net buoyancy flux, so either smaller volumes of higher salinity waters are needed (with strong ambient deep-water entrainment), or larger volumes of less saline waters (with less entrainment); either way, the mass-weighted salt and $\delta^{18}O$ flux will be roughly similar. If such events took place, then we expect anomalies with elevated temperatures and higher δ_w, and cancelation effects between these two influences would result in muted δ_c changes. Our δ_c-based sea-level reconstruction would then indicate little sea-level change, as would the related $\Delta_{\delta w}$. With muted δ_c and δ_w changes, δ_c residuals would also be small, and we would, thus, infer little T_w change. We find no intervals with muted variance in all three parameters (Δ_{SL}, δ_w, and T_w). We therefore infer that there is no evidence for periods of dominant warm, saline deep-water contributions throughout the timescales investigated.

Supplementary Figures

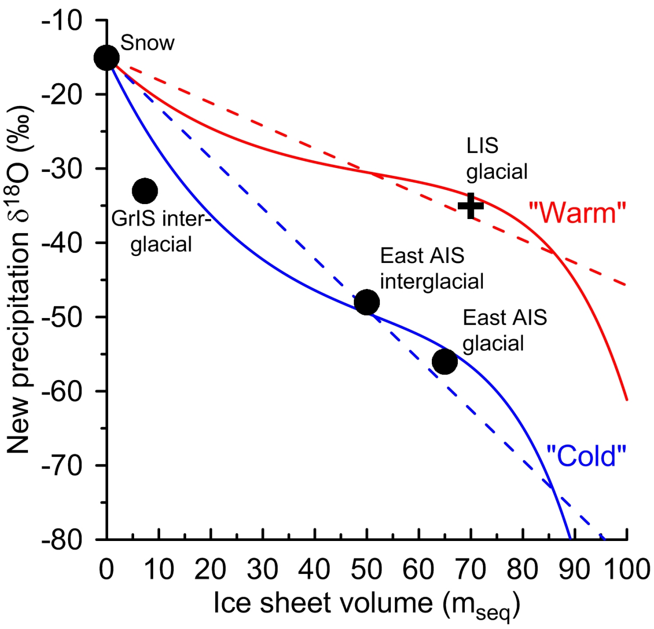

Supplementary Figure S1. Shape of the δ_p *versus* ice-sheet volume relationships used in our analytical and applied assessments. Blue indicates lines used for AIS and GrIS ("cold" high-latitude ice sheets), and red lines are used for LIS and EIS ("warm" lower-latitude ice sheets). Solid lines are heuristically fitted function shapes discussed in Methods. Dashed lines are the linear relationships used in sensitivity test 1 of the analytical assessment (Methods). Heavy dots are control values for snow (see main text), interglacial GrIS (*41*) (glacial GrIS is not used because of uncertainty about the amount of excess glacial ice), and modern and glacial eastern EIS (*42*). The cross indicates a LGM value for LIS of roughly –35 ‰ based on isotope-enabled global climate circulation models (*35*). The fits are approximations because there are not enough data for a robust fit. However, the analytical assessment indicates that the function shape used here has little impact on our conclusions (Fig. 1).

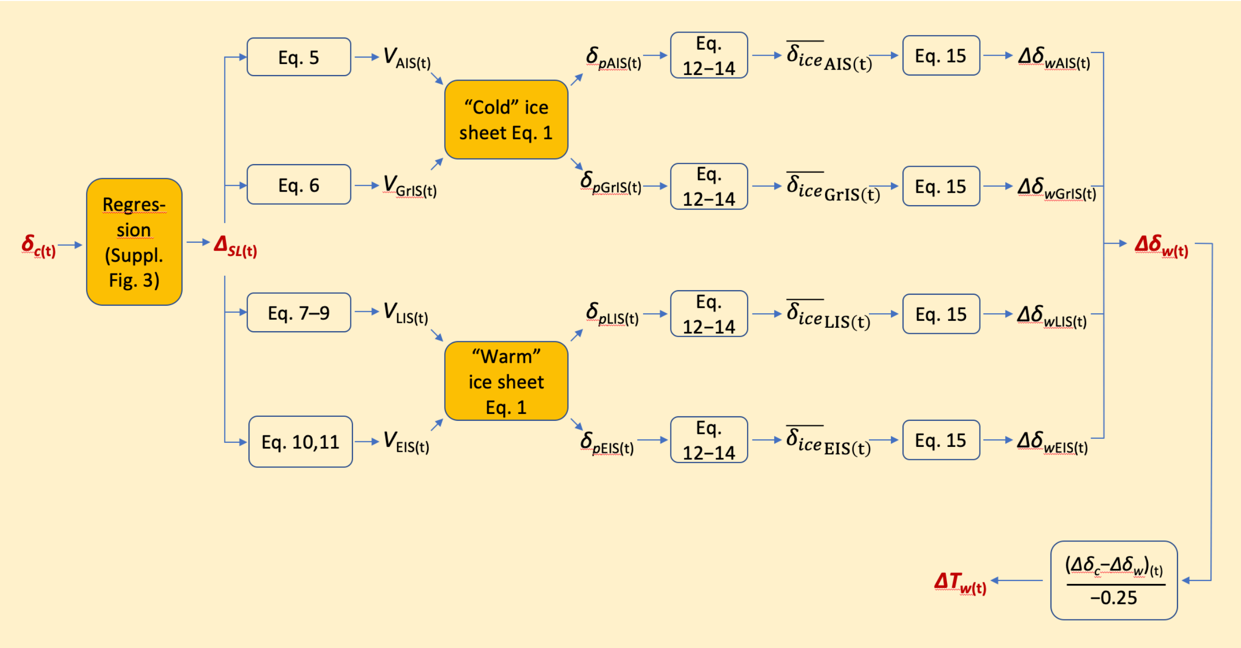

Supplementary Figure S2. Diagram of the workflow used in our applied assessments. Equation numbers refer to the Methods section. Subscript (t) is given to indicate parameter development through time. Red highlights indicate the main parameters of interest between which we investigate mutually consistent relationships. It is evident from the left-to-right progression that there are no circularities in the method. Darker yellow boxes indicate stages where the main assumptions are made. One assumption concerns the regression-based approach to derive Δ_{SL} from δ_c (Suppl. Fig. S3). Sensitivity tests with different regressions indicate that the Δ_{SL} solution is robust within a total uncertainty range of about 10 m (i.e., if a mean were chosen from the three solutions, then uncertainties would span up to ±5 m at 99% confidence). This robustness is emphasized by the multi-parameter validations undertaken here. Another assumption concerns the shape of the δ_p relationships with ice volume. Sensitivity tests with alternative contrasting (linear) relationships indicate that our main conclusions are affected little by the relationship shape (Fig. 1).

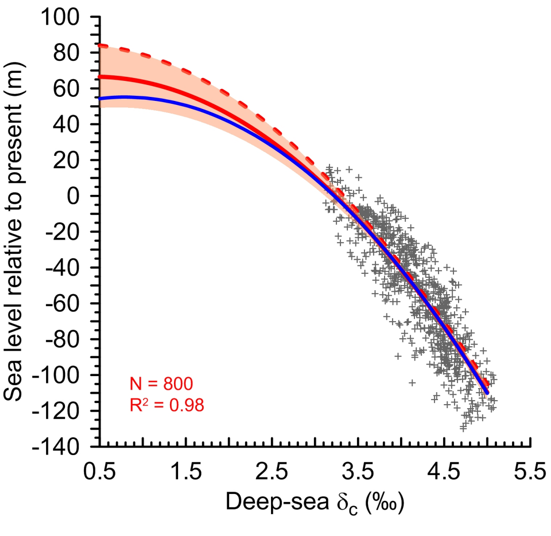

Supplementary Figure S3. Lag-optimized (*12*) regressions between the benthic foraminiferal carbonate δ^{18}O stack (*13*) and sea-level (*12*). Second order polynomials are used (*12*). The solid red line is our main-case conversion regression, which is constrained to peak at 65.1 m. The shaded band indicates its 95% confidence interval, which includes both uncertainty in the regression through the dataset, and normally distributed uncertainties in both *X* and *Y* directions for all data points, with 1σ = 0.1 ‰ for δ_c and 1σ = 2 m for Δ_{SL}. For an upper extreme, we use the upper 95% line (dashed red). For a lower extreme, we use the unconstrained second-order polynomial (solid blue). This line peaks at about 55 m and, thus, always "leaves" about 10 m of ice, which is unrealistic. Thus, we ignored the lower 95% bound of the main regression because that remains even lower. Main line equation (solid red): $\Delta_{SL} = -8.4\ \delta_c^2 + 6.8\ \delta_c + 65.1$. Upper 95% bound equation (dashed red): $\Delta_{SL} = -7.8\ \delta_c^2 + 0.1\ \delta_c + 86.2$. Unconstrained polynomial equation (solid blue): $\Delta_{SL} = -9.3\ \delta_c^2 + 14.3\ \delta_c + 50.4$. Statistics given in the figure refer to the main polynomial.

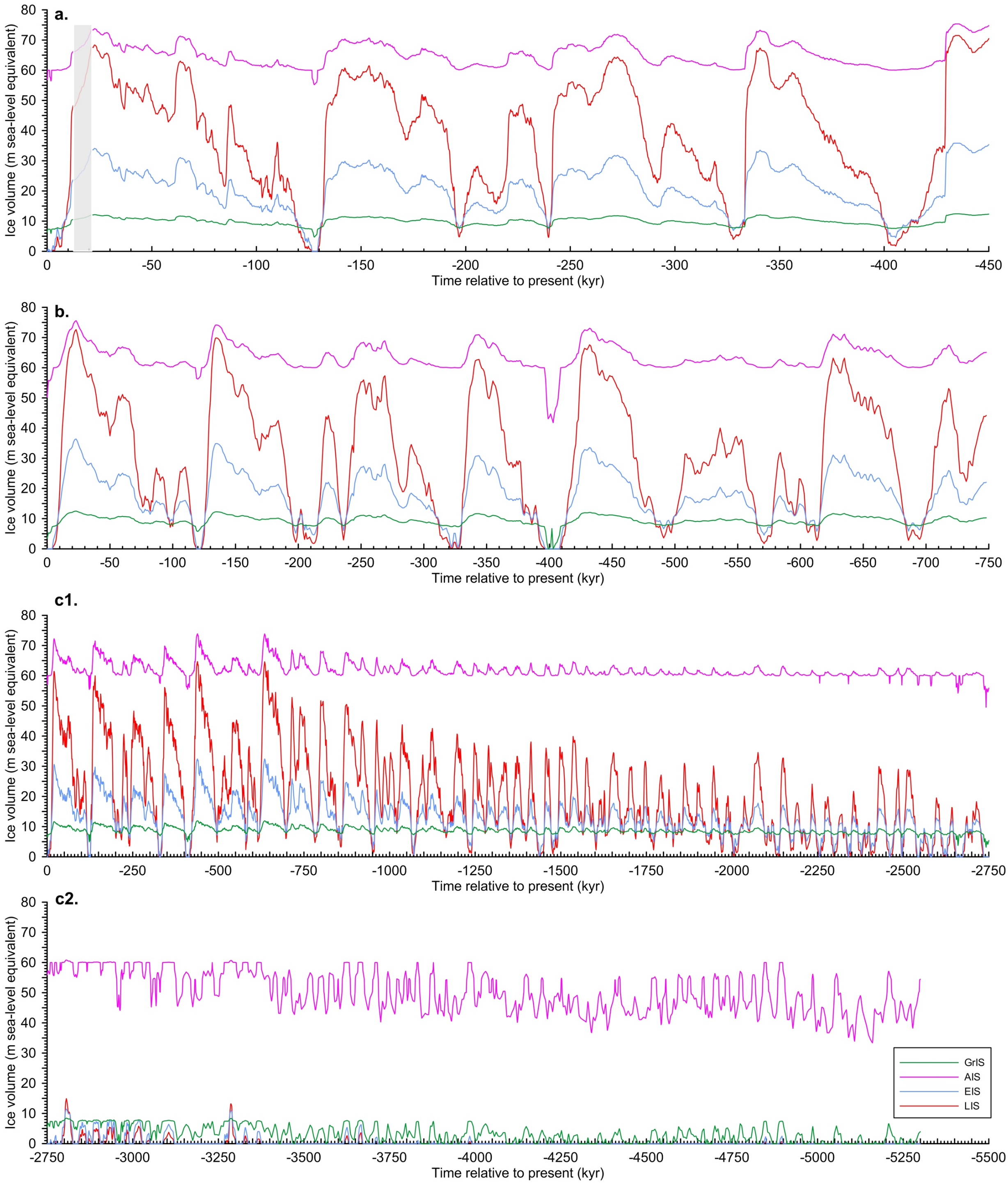

Supplementary Figure S4. Volumes of the various ice sheets. For sea level based on: **a.** the Red Sea record (*8,9,10,11*); **b.** sea-level stack (*12*); **c1** and **c2.** the benthic δ_c stack (*13*) (main case regression, Suppl. Fig. S3). Panel **c** is divided into younger (**c1**) and older (**c2**) halves, for clarity.

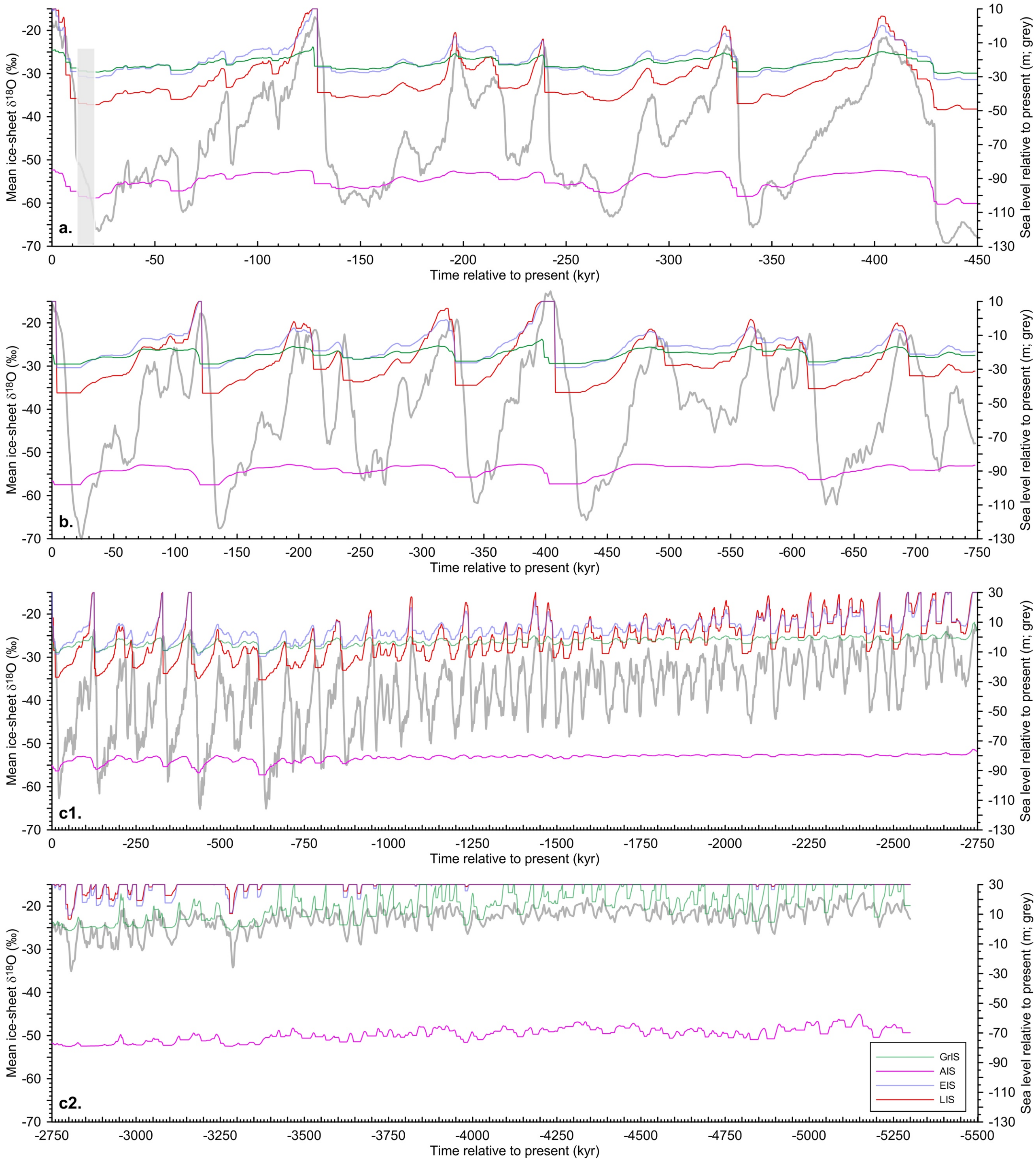

Supplementary Figure S5. Weighted mean ice-sheet δ18O for the various ice sheets ($\overline{\delta_{ice}}$). For sea level based on: **a.** the Red Sea record (*8,9,10,11*); **b.** sea-level stack (*12*); **c1** and **c2.** the benthic δ_c stack (*13*) (main case regression, Suppl. Fig. 3). Panel **c** is divided into younger (**c1**) and older (**c2**) halves, for clarity.

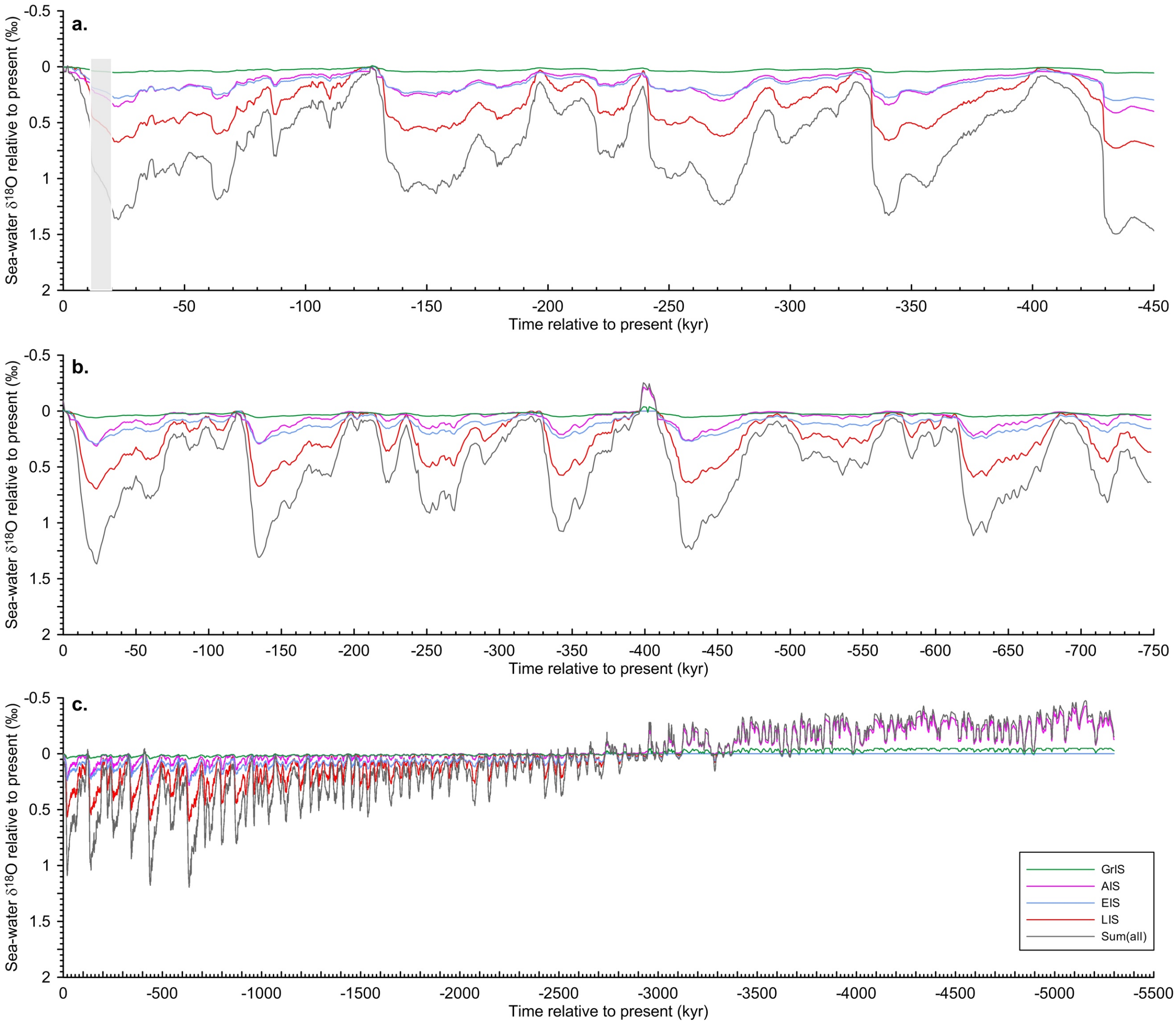

Supplementary Figure S6. Imposed changes to sea-water $\delta^{18}O$ (i.e., $\Delta\delta_w$) by individual ice sheets, and their combined impact. For sea level based on: **a.** the Red Sea record (*8,9,10,11*); **b.** sea-level stack (*12*); **c1** and **c2.** the benthic δ_c stack (*13*) (main case regression, Suppl. Fig. 3). Panel **c** is divided into younger (**c1**) and older (**c2**) halves, for clarity.

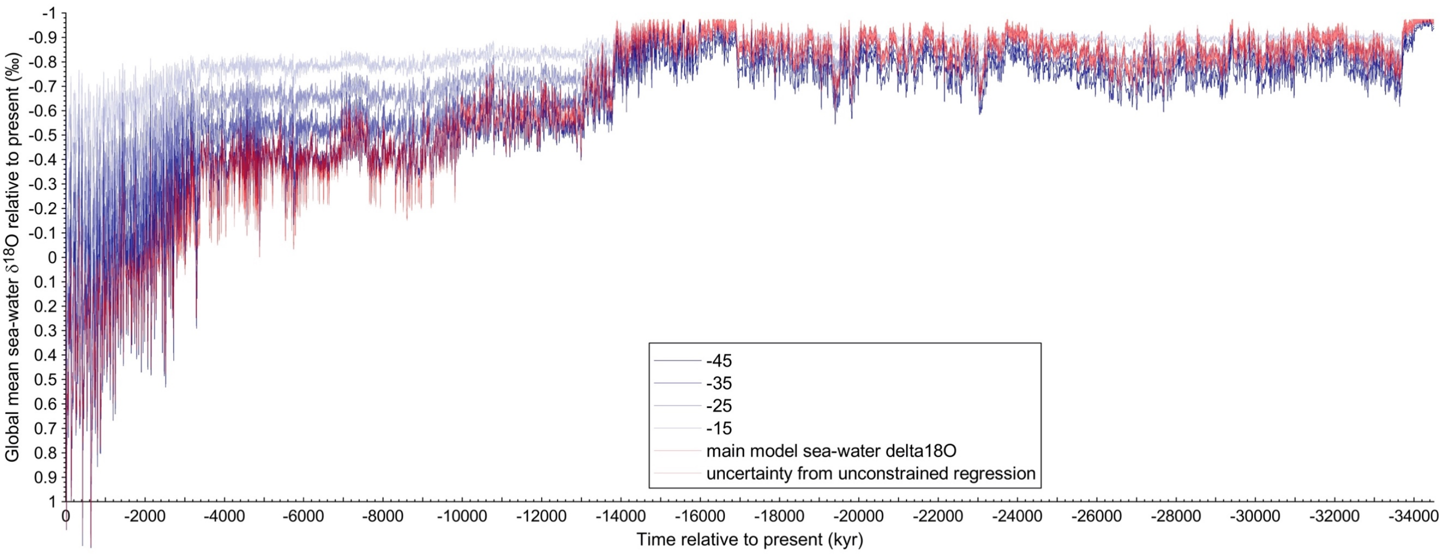

Supplementary Figure S7. Sea-level related change in sea-water δ^{18}O (i.e., $\Delta\delta_w$). Blue lines reflect reconstructions from $\Delta\delta_w$:Δ_{SL} relationships based on different mass-weighted mean global δ_{ice} values (δ_{ice}^*), as specified in the legend (‰). Red lines with shading in between indicate results from the model presented here (regression range as specified in the legend). For ice-volume growth indicated by our regression-based Δ_{SL} record (Suppl. Fig. S3), Rayleigh-distillation based fractionation of δ_p for AIS at the EOT evolves rapidly to –30 to –35‰. Assuming more negative initial snow δ_p but similar δ_p development for a large-size AIS (i.e., adjusting the intercept in the relationship for AIS in Suppl. Fig. 1) only negligibly shifts the red curve because the ice sheet grows rapidly to mid-size dimensions. Hence, such an assumption yields no feasible solution to the limited δ_w impact of AIS growth at the EOT.

Supplementary Table S1. Details of information included in the Red Sea, Mediterranean, and statistical sea-level reconstructions.

Record	Process	Input	References
Red Sea	Residence-time model based on hydraulic control at the sill connecting the Red Sea to the open ocean	Multi-source δ_c stack	*8,9,10,11*
Mediterranean Sea	Residence-time model based on hydraulic control at the sill connecting the Mediterranean Sea to the open ocean	Planktonic δ_c stack	*46*
Statistical sea-level record	1st Principal Component (all sources had roughly equal loading)	1. Global planktonic δ_w synthesis 2. Atlantic benthic δ_w 3. Benthic δ_c regression to corals 4. Pacific benthic δ_w 5. Mediterranean RSL 6. Red Sea RSL 7. Inverse model	*12*